

To appear in *The Astronomical Journal*, Vol. 132, July 2006

## Far-flung Filaments of Ejecta in the Young Supernova Remnant G292.0+1.8

P. Frank Winkler<sup>1</sup>

*Department of Physics, Middlebury College, Middlebury, VT 05753*

winkler@middlebury.edu

and

Knox S. Long<sup>1</sup>

*Space Telescope Science Institute, 3700 San Martin Drive, Baltimore MD 21218*

long@stsci.edu

### ABSTRACT

New optical images of the young supernova remnant (SNR) G292.0+1.8, obtained from the 0.9-m telescope at CTIO, show a more extensive network of filaments than had been known previously. Filaments emitting in [O III] are distributed throughout much of the 8 arcmin diameter shell seen in X-ray and radio images, including a few at the very outermost shell limits. In addition to the extensive [O III] filaments, we have detected four small complexes of filaments that show [S II] emission along with the oxygen lines. In a single long-slit spectrum we find variations of almost an order of magnitude in the relative strengths of oxygen and sulfur lines, which must result from abundance variations. None of the filaments, with or without [S II], shows any evidence for hydrogen, so all appear to be fragments of pure supernova ejecta. The [S II] filaments provide the first evidence for undiluted products of oxygen burning in the ejecta from the supernova that gave rise to G292.0+1.8. Some oxygen burning, either hydrostatic or explosive, must have occurred, but the paucity of [S II]-emitting filaments suggests that either the oxygen burning was not extensive or that most of its products

---

<sup>1</sup>Visiting Astronomer, Cerro Tololo Inter-American Observatory. CTIO is operated by AURA, Inc. under contract to the National Science Foundation.

have yet to be excited. Most of the outer filaments exhibit radial, pencil-like morphologies that suggest an origin as Rayleigh-Taylor fingers of ejecta, perhaps formed during the explosion. Simulations of core-collapse supernovae predict the development of such fingers, but these have never before been so clearly observed in a young SNR. Following careful subtraction of the stars in the field, we have measured the total flux in [O III]  $\lambda$  5007 as  $5.4 \times 10^{-12}$  ergs cm $^{-2}$  s $^{-1}$ . Using a distance of 6 kpc and an extinction correction corresponding to  $E(B - V) = 0.6$  mag (lower than previous values but more consistent both with our data and with X-ray and radio measurements of the hydrogen column density) leads to a luminosity of  $1.6 \times 10^{35}$  ergs s $^{-1}$  in the 5007 Å line.

*Subject headings:* ISM: individual (SNR G292.0+1.8) — nuclear reactions, nucleosynthesis, abundances — shock waves — supernova remnants

## 1. Introduction

The canonical picture of a supernova remnant (SNR) that results from the core collapse and supernova explosion of a massive star includes a shell produced by an expanding shock, fragments of ejecta that may appear as optical filaments rich in oxygen and (often) other heavy elements, a central neutron star that manifests itself as a pulsar, and a synchrotron-emitting pulsar wind nebula that surrounds and is powered by the pulsar. Yet there is only a single SNR in the Galaxy that has been found to display all these properties: G292.0+1.8, also known as MSH 11–54, and its associated pulsar PSR J1124–5916 (Hughes et al. 2001; Camilo et al. 2002; Hughes et al. 2003). This system thus provides a unique opportunity to study both the compact and ejected remains from a massive star and their interaction with the local environment.

Although G292.0+1.8 (henceforth more succinctly G292) was originally detected and identified as a SNR through its radio properties (Mills et al. 1961; Milne 1969), it first attracted significant attention when Goss et al. (1979) discovered optical filaments with spectra dominated by lines of oxygen and neon. Hydrogen Balmer lines, and also lines of [S II] and [N II] typically seen in SNRs, were conspicuous by their absence. Murdin & Clark (1979) showed these filaments to have high radial velocities,  $-700$  km s $^{-1} \lesssim v_{\text{rad}} \lesssim +1300$  km s $^{-1}$ , indicating that they are undecelerated (or minimally decelerated) ejecta from the supernova explosion. G292 thus joined the prototype Cas A in the class of “oxygen-rich” SNRs—an exclusive group that still comprises only about 8 members. The optical filaments with extremely metal-rich spectra that characterize the O-rich remnants are fragments of nearly pure ejecta that were launched from the core of the progenitor star during its explosion and

that remain virtually uncontaminated through interaction with interstellar or circumstellar material. Subsequent spectra of G292 by Dopita & Tuohy (1984) and Sutherland & Dopita (1995a) have shown no lines other than those of oxygen and neon.

G292 has been the subject of numerous X-ray studies, culminating in the spectacular high-resolution image from *Chandra* (Park et al. 2002). The X-ray spectrum is dominated by K-shell lines of O, Ne, Mg, Si, and S. Non-equilibrium ionization analyses require large enhancements (relative to solar) in abundances for O, Ne, and Mg, with lesser enhancements for Si, S, and Fe (Hughes & Singh 1994; Gonzalez & Safi-Harb 2003). By comparing the inferred abundances with the integrated yields predicted by models for core-collapse supernovae, they estimated a progenitor mass of  $\sim 20 - 40 M_{\odot}$ . In a more detailed study of individual X-ray features, Park et al. (2004) found that different knots have very different compositions and suggested that these represent clumps of ejecta from different zones of the progenitor.

The *Chandra* image of G292 also revealed a compact central source, surrounded by what appeared to be a pulsar wind nebula (Hughes et al. 2001). Shortly thereafter, Camilo et al. (2002) discovered the radio pulsar PSR J1124–5916 within or very near G292. Hughes et al. (2003) then showed that the compact X-ray source is pulsed with the same period, confirming that it must be the compact remnant of the star that produced G292. The period of 135 ms and spin-down age of 2900 yr are roughly consistent with the age of the G292 SNR, estimated by Chevalier (2005) as 2700–3700 yr based on properties of the pulsar-wind nebula, and more directly as 3000–3400 yr from the kinematic study by Ghavamian et al. (2005).

Detailed radio images of G292 obtained by Gaensler & Wallace (2003) show a bright central core around the pulsar, surrounded by a fainter plateau about  $8'$  in diameter with sharp outer edges. The outer edge of the radio plateau coincides closely with the outer extent of X-ray emission seen in the *Chandra* image, and must delineate the SNR’s primary shock. Based primarily on the H I absorption profile, Gaensler & Wallace (2003) also give what is probably the most reliable distance estimate to G292:  $6.2 \pm 0.9$  kpc, which implies a diameter of about 15 pc for the SNR.

In this paper we present the first CCD images that cover the full extent of G292. The narrow-band [O III] image, especially after we subtract a matched continuum image, shows a network of filaments far more extensive than indicated in photographic studies (Goss et al. 1979; Tuohy et al. 1982), and even more wide-spread than those in the Fabry-Perot studies of Ghavamian et al. (2005). In addition, we have discovered a few filaments that show emission lines of [S II] in addition to oxygen and neon—the first evidence for the presence of oxygen-burning products in the ejecta-dominated optical filaments.

## 2. Emission-Line Images

We have obtained optical images of G292 in emission lines of [O III], [S II], and  $H\alpha$ , along with matched red and green continuum bands, from CTIO using the 0.9-m telescope and Tek2K no. 5 CCD on 2002 March 20 and 23 (UT). The continuum bands are important since they enable us to subtract away most of the light from the numerous stars that litter this dense Galactic field to reveal faint, small scale emission features of the SNR itself. The  $2048 \times 2048$  pixel chip covered a field  $13'.8$  square at a scale of  $0''.401 \text{ pixel}^{-1}$ , easily accommodating the  $\sim 8'$  diameter of G292. We were favored with photometric conditions and seeing about  $1''$  throughout the run, and all the G292 images were taken with no moon. We obtained 3 to 5 frames in each filter and dithered the telescope by a few arcsec between frames to paper over cosmetic defects and to minimize systematic effects of chip sensitivity.

Details of the observations are given in Table 1. The images were processed using standard IRAF<sup>1</sup> procedures of bias-subtraction and flat-fielding. Flux calibration was achieved through observation of spectrophotometric standard stars from the list of Hamuy et al. (1992) each night during the run. All the images were aligned to a common coordinate system using some 300 stars from the UCAC1 catalog (Zacharias et al. 2000).

The combined [O III] image is shown in Fig. 1, both before (Fig. 1a) and after (Fig. 1b) continuum subtraction. Although artifacts of many bright stars remain, the faint emission features are far more evident in the continuum-subtracted image. In Fig. 2 we compare our [O III] image of G292 with an X-ray image from the *Chandra* ACIS-S image on the same scale. (These data, obtained from the *Chandra* archive, are the same as those used by Park et al. (2002) for their color image.) We have placed matching contours on both images to clarify the relative locations of X-ray and optical features.

It is apparent from these CCD images that the [O III]-emitting filaments in G292 are far more numerous and more extensive than early photographic images (Goss et al. 1979; Tuohy et al. 1982)<sup>2</sup> indicated. Not surprisingly, features in the central region coincide with those shown in the Fabry-Perot images of Ghavamian et al. (2005), but our images also show many filaments near the periphery of the shell, outside their Fabry-Perot field. In addition to the bright crescent-shaped group of filaments east of the X-ray center, sometimes referred to as the “spur,” fainter individual knots and more diffuse filaments are present throughout

---

<sup>1</sup>IRAF is distributed by the National Optical Astronomy Observatories, which is operated by the AURA, Inc. under cooperative agreement with the National Science Foundation.

<sup>2</sup>When comparing our images with those of Goss et al. (1979), note that their Plate 1 is reproduced as a mirror image to the conventional north up, east left orientation.

much of the  $8'$  diameter of the X-ray remnant.

It might at first appear that the southernmost optical filaments, located near  $\alpha(2000) = 11^{\text{h}}24^{\text{m}}29^{\text{s}}$ ,  $\delta(2000) = -59^{\circ}20'38''$ , lie outside the X-ray shell. This is not the case; these filaments simply lie outside the field covered by the ACIS-S3 chip. X-ray images from the *ROSAT* HRI (unpublished archive data), which cover a wider field than the ACIS image (though with lower sensitivity and angular resolution), show a diffuse X-ray extension at the southern extreme of the G292 shell. We have added the outer contours from the *ROSAT* image to Fig. 2b in order to show the full extent of X-ray structure. Still, the southernmost [O III] filaments appear to lie very near the outer extreme of even this extended X-ray emission.

In addition to the extensive network of filaments seen in the [O III] images, we have also detected a few filaments in [S II]  $\lambda\lambda$  6716, 6731. Our [S II] images show at least four faint individual filaments or small complexes, illustrated in Fig. 3. These represent the first evidence for the presence of sulfur, or of any of the Si-group elements that result from O-burning, in optical filaments of G292. Though clear and unambiguous, the [S II] emission is significantly fainter than that in [O III]. The brightest [O III] filament is the northern portion of the spur, which runs nearly E-W centered at  $\alpha(2000) = 11^{\text{h}}24^{\text{m}}48^{\text{s}}.7$ ,  $\delta(2000) = -59^{\circ}15'41''$ . In the very brightest area of this filament the [O III] intensity is  $2.8 \times 10^{-15} \text{ ergs cm}^{-2} \text{ s}^{-1} \text{ arcsec}^{-2}$ , more than 20 times the [S II] intensity at the same location. An extension of Filament 1, located  $\sim 18''$  to the west and designated 1W in Fig. 3, has  $I_{[\text{S II}]} = 0.5 \times 10^{-15} \text{ ergs cm}^{-2} \text{ s}^{-1} \text{ arcsec}^{-2}$ , while  $I_{[\text{O III}]} = 1.6 \times 10^{-15} \text{ ergs cm}^{-2} \text{ s}^{-1} \text{ arcsec}^{-2}$  is now only 3 times brighter. The slit for the spectrum presented in §3 was oriented to cover both the above portions of Filament 1, designated 1 East and 1 West, as shown in detail in Fig. 5.

The brightest of the [S II] filaments is the one designated 3 in Fig. 3, and located at  $\alpha(2000) = 11^{\text{h}}24^{\text{m}}39^{\text{s}}.8$ ,  $\delta(2000) = -59^{\circ}12'36''$ . Marginally resolved in our images, it has  $I_{[\text{S II}]} \approx 1.0 \times 10^{-15} \text{ ergs cm}^{-2} \text{ s}^{-1} \text{ arcsec}^{-2}$ , more than twice  $I_{[\text{O III}]}$  at the same location. There are no spectra of this filament as yet.

We can estimate the integrated [O III] flux from the entire remnant by summing the flux in each of the regions containing filaments, to obtain  $F_{5007} \approx 5.4 \times 10^{-12} \text{ ergs cm}^{-2} \text{ s}^{-1}$ , with an uncertainty which we estimate as  $\sim 20\%$ . The myriad stars in the field contribute many times more (continuum) flux in the 60-Å bandpass than the line flux from the filaments, so imperfect star subtraction can lead to a significant error in the nebular flux. With this caveat we give our result, since we know of no previous values for such a quantity from G292.

Finally, we have also obtained an image in  $\text{H}\alpha$ , shown in Fig. 4. All of the fine filaments

seen in [O III] or [S II] are completely absent in H $\alpha$ . There is a considerable amount of faint diffuse H $\alpha$  structure, virtually all of which also appears even more faintly in [S II] (Fig. 3). Figure 9 of Ghavamian et al. (2005) shows the H $\alpha$  emission in the central region of G292 more clearly, and these authors further show that all the H $\alpha$  is at essentially zero radial velocity, quite unlike the [O III] filaments. They speculate that the H $\alpha$  structures may result from interstellar or circumstellar material in the vicinity of G292 that has been excited either by slow shocks or by photoionization caused by the strong radiative shocks that produce the X-ray emission. Looking at these structures in a larger context, however, shows that diffuse structures seen in both H $\alpha$  and [S II], very similar to ones within G292, extend well beyond the boundary of the SNR shell. It is entirely possible that this diffuse emission may not be related to G292 at all. Not surprisingly, there is considerable diffuse H $\alpha$  emission on a much larger scale throughout this field near the Galactic plane. The SHASSA survey (Gaustad et al. 2001) shows a band of diffuse emission passing roughly NE to SW through G292, with  $I_{\text{H}\alpha} \sim 80$  to 90 Rayleigh (averaged over the  $0.8 \text{ pixel}^{-1}$  resolution of that survey), equivalent to an emission measure of  $180\text{--}200 \text{ cm}^{-6} \text{ pc}$ . The intensity of the brightest diffuse H $\alpha$  within the G292 shell is  $I_{\text{H}\alpha} = 0.6 \times 10^{-15} \text{ ergs cm}^{-2} \text{ s}^{-1} \text{ arcsec}^{-2} = 110 \text{ Rayleigh}$ , which represents little if any enhancement over the diffuse Galactic emission seen throughout the region. The question of whether or not the H $\alpha$  emission is physically associated with G292 may eventually be resolved through observations from *Spitzer*, since one would expect mid-infrared radiation from dust grains heated by the passage of a strong SNR shock.

Since the ejecta-dominated filaments are known to have high velocities, the pass bands of the filters are important, and the velocity ranges are included in Table 1. The [O III] filter admits emission in the velocity range  $-1700$  to  $+1800 \text{ km s}^{-1}$ , easily encompassing the full range for which emission has been reported for G292 by Ghavamian et al. (2005) or any previous studies. The [S II] image should include emission in one or both lines of the  $\lambda\lambda 6716, 6731$  doublet from material in the range  $-1200$  to  $+1600 \text{ km s}^{-1}$ , but it is possible that extremely blue-shifted [S II] emission might have fallen largely outside the pass band of our filter. The same is true for H $\alpha$ , of course, where the pass band is narrower ( $-450$  to  $+650 \text{ km s}^{-1}$ ), but neither we nor Ghavamian et al. (2005) see any evidence for H $\alpha$  emission from any of the fast, ejecta-dominated filaments.

### 3. Long-slit Spectroscopy

We obtained deep spectra of filament 1, the brightest filament in G292, from the CTIO 1.5m telescope and R-C spectrograph in 1997 March.<sup>3</sup> A slit of width  $3''.5$  ( $193.5 \mu$ ) was aligned at a position angle of  $100^\circ.5$  as shown in Fig. 5, in order to capture the brightest portion of the [O III] and the [S II] emission in spatially distinct regions along the slit. Three different spectrograph setups were used, as detailed in Table 2. All used 300 line/mm gratings to give a dispersion of  $2.9 \text{ \AA pixel}^{-1}$ . The observations using the red and IR setups were carried out on the night of 1997 March 28 (U.T.), and those in the blue setup were done the following night. We were careful to adjust the slit position and orientation to be virtually identical for all three spectra.

Data reduction was carried out using IRAF and following standard CTIO procedures for this spectrograph: initial flat-fielding using dome flats (combined with an internal quartz-lamp flat for the blue setup only) was followed by slit-illumination correction using well-exposed twilight sky flats. Comparison spectra using a HeNeAr lamp were obtained both before and after each sequence of observations for wavelength calibration. For flux calibration we used several stars from the Hamuy et al. (1992) list, observed over a range of airmasses.

The two-dimensional spectrum from the red setup is shown in Fig. 6. Emission from Filament 1 shows a similar characteristic curvature in each of several emission lines, the result of a radial velocity gradient along the filament. The complete absence of any  $H\alpha$  emission showing a similar velocity profile constitutes further evidence that this filament is composed almost entirely of heavy elements, i.e., supernova ejecta. Close inspection of the figure shows that the 2-dimensional emission pattern is virtually identical in lines of [O I], [O II], and [O III], but that the [S II] lines show a somewhat different pattern. All of the oxygen lines are strongest toward the eastern end of the filament (toward the bottom in Fig. 6), while the [S II] lines are strongest in the west. This is exactly what one expects from comparing the images in [O III] and [S II] (Fig. 5).

Fig. 7 shows a pair of one-dimensional spectra obtained by summing over several rows in two regions along the slit: one to the east where the oxygen lines are strongest (denoted 1E in Fig. 6), and the other to the west where the [S II] lines are strongest (denoted 1W). These one-dimensional data shown in Fig. 7 are actually the combination of spectra extracted from identical regions of all three spectrograph setups. (We do not show the spectrum at  $\lambda > 8000 \text{ \AA}$ , since no lines emerge above the noise at these wavelengths.) Furthermore, we

---

<sup>3</sup>This was 5 yr prior to the run during which the image data presented in §2 were obtained. We had found evidence for [S II] emission during an earlier imaging observation that covered only the central region of G292 and had poorer seeing than the images shown in §2.

applied a transformation to artificially “straighten” the spectra before extraction, in order to avoid broadening the lines by summing emission from material at different velocities. The line fluxes in the spectra of the two regions are tabulated in Table 3.

There has been no optical spectroscopy of G292 capable of yielding an unambiguous determination of the reddening, but virtually all of the scant literature describing G292’s optical emission has adopted the value of  $E(B-V) = 0.9$  mag proposed by Goss et al. (1979). We argue in §4.2 that spectra both in the optical and in other bands are best interpreted by using a smaller value,  $E(B-V) \approx 0.6$  mag. In Table 3 we give dereddened intensities for both these values of  $E(B-V)$ , where we have used the extinction function of Cardelli et al. (1989) with  $A(V)/E(B-V) = 3.1$ .

Although oxygen lines clearly dominate the spectrum from both regions, the [S II] lines are stronger *relative to the oxygen lines* by about a factor of 8 in the western (upper) spectrum when compared with the eastern (lower) one. The relative strengths of the [O I], [O II], and [O III] lines are similar in the two spectra, therefore we can exclude the possibility that the variation in S/O line strengths along the filament results from some difference in physical conditions. Instead, variations in the S/O abundance ratio must be responsible. Furthermore, note that in the east the [S II] lines suggest an electron density near the low-density limit, while the much stronger [S II] lines in the west indicate  $n_e \sim 200 \text{ cm}^{-3}$ .

Finally, we note that in addition to the numerous forbidden lines of oxygen, *permitted* O I  $\lambda 7774$  is also present. This is a recombination line, and the fact that it is not just present, but stronger than  $H\alpha$ , indicates that  $O^+$  is winning out over  $H^+$  in the competition for recombination electrons; i.e., that oxygen is more abundant than hydrogen. The same line has been observed in other oxygen-rich SNRs such as Puppis A (Winkler & Kirshner 1985), Cas A (Winkler et al. 1991; Hurford & Fesen 1996), and the SMC remnant E0102.2–7219 (Blair et al. 1989).

## 4. Discussion

### 4.1. Reddening, Spectral Diagnostics, and [O III] Luminosity

Goss et al. (1979), in the paper where G292 was first identified as an oxygen-rich SNR, estimated that the reddening was  $E(B-V) = 0.9$  mag, arguing for consistency in the relative strengths of the oxygen lines. Although this argument depends entirely on highly uncertain models for the emission from shocked material composed almost entirely of metals, this original value for the reddening has persisted in the literature. An alternative approach to obtaining the reddening is through the hydrogen column density,  $N_H$ , which Predehl &



Schmitt (1995) have shown to be closely correlated with optical extinction. They found that these quantities to be related by  $N_H/A_V = 1.79 \times 10^{21} \text{ cm}^{-2}\text{mag}^{-1}$ , equivalent to  $E(B - V) = 5.55 \times 10^{21} \text{ cm}^{-2}\text{mag}^{-1}$ .

There have been a number of recent measurements of  $N_H$  based on X-ray and radio data. Gonzalez & Safi-Harb (2003) found a value  $(5 \pm 1) \times 10^{21} \text{ cm}^{-2}$  based on an average of fits to the spectra from numerous X-ray knots in G292, suggesting  $E(B - V) = 0.9 \pm 0.2$  mag. Park et al. (2004) fit the spectra of a number of individual X-ray knots and found values for  $N_H$  ranging from 3 to  $7.7 \times 10^{21} \text{ cm}^{-2}$ , equivalent to  $E(B - V)$  from 0.5 to 1.4 mag. However, modeling of thermal X-ray plasmas with abundances that may be far from solar is difficult, and the absolute accuracy of fits based on these models is hard to assess. For this reason, we believe the most reliable X-ray determination of the column density is that by Hughes et al. (2001), who fit the pulsar spectrum with an absorbed power law to obtain  $N_H \approx (3.17 \pm 0.15) \times 10^{21} \text{ cm}^{-2}$ , close to the minimum value derived by Park et al. (2004). This lower value agrees well with the column obtained using radio data by Gaensler & Wallace (2003), who integrated the H I emission over a range of velocities and inferred that  $N_H \approx 3.3 \times 10^{21} \text{ cm}^{-2}$ , equivalent to  $E(B - V) = 0.6$  mag.

The most successful models for the optical emission from young, oxygen-rich SNRs are those of Sutherland & Dopita (1995b), who calculated the emission resulting when a strong (reverse) shock enters an oxygen-rich fragment of material from a progenitor core. They considered both direct post-shock emission and also the indirect effects of X-rays that can produce an ionization front propagating into the fragment ahead of the shock itself. They used a grid of models considering either or both of these processes, with a range of shock velocities, and calculated diagnostic ratios for various oxygen lines. Comparing their models with our observed spectra, we find that dereddening as much as  $E(B - V) = 0.9$  leads to intensities for [O II]  $\lambda$  3727 that are stronger than any of their models predict. Sutherland & Dopita (1995b) had precisely the same problem for G292, and indeed their own observed intensity ratios (from Sutherland & Dopita 1995a, where they also used  $E(B - V) = 0.9$ ) are almost exactly the same as ours for the bright Filament 1 East. But decreasing the reddening to  $E(B - V) = 0.6$  gives ratios very similar to their model OSP150, which includes both direct post-shock emission and preionization from a  $150 \text{ km s}^{-1}$  shock, and also similar to ratios they report for a number of filaments in the O-rich remnant N132D in the Large Magellanic Cloud. For example, the most reddening-sensitive ratio in their analysis is [O II]  $\lambda$  7325:[O II]  $\lambda$  3727. For  $E(B - V) = 0.6$ , our dereddened intensity ratio for both the East and West regions of Filament 1 (see Table 3) is 0.028, almost exactly that predicted by the OSP150 model, while for  $E(B - V) = 0.9$  it is half this value and substantially lower than has been observed in dereddened spectra of other O-rich SNRs (see e.g. Sutherland & Dopita 1995b, Fig. 13c).

Here and in the subsequent discussion we adopt the value  $E(B - V) = 0.6$  mag, which is consistent with most X-ray and radio measurements of the column density and gives relative line strengths that are consistent with the best models for a plasma composed entirely of heavy elements. This in turn allows us to estimate the luminosity of G292 in  $[\text{O III}] \lambda 5007$ . Using our estimate (§ 2) of the integrated flux,  $F_{5007} = 5.4 \times 10^{-12}$  ergs cm $^{-2}$  s $^{-1}$ , and our adopted value for the extinction implies  $L_{5007} = 1.6 \times 10^{35} d_6^2$  ergs s $^{-1}$ , where  $d_6$  is the distance modulo 6 kpc. This luminosity value has an uncertainty  $\sim 20\%$  attributable to our flux estimate, in addition to any uncertainty in the extinction.

One other O-rich SNR for which the  $[\text{O III}]$  luminosity has been reported is the extremely bright SNR in the Magellanic-type irregular galaxy NGC 4449, at a distance of about 3.9 Mpc (Hunter et al. 1999). For this case Blair et al. (1983)<sup>4</sup> give  $F_{4959+5007} = 2.02 \times 10^{-13}$  ergs cm $^{-2}$  s $^{-1}$ . If we attribute 3/4 of the total flux to the 5007 Å line and correct after for extinction we find  $L_{5007} = 5.2 \times 10^{38}$  ergs s $^{-1}$ , 300 times higher than G292. It has been recognized since its discovery, however, that the NGC 4449 SNR is extraordinary; its X-ray and radio luminosities are also higher than any other known remnants. It should be straightforward to obtain  $[\text{O III}]$  luminosities for most or all of the other O-rich SNRs, but no values are readily available in the literature.

#### 4.2. $[\text{S II}]$ Emission and Nucleosynthesis Implications

The detection of  $[\text{S II}]$  emission, even if in only a handful of filaments, is nevertheless significant. Sulfur resulting from massive-star supernovae stems almost entirely from oxygen burning, either hydrostatically in a shell surrounding the core during a short time before core collapse, and/or explosively during the supernova itself (e.g. Arnett 1996; Woosley et al. 2002). The presence of S in fragments of pure SN ejecta (which these filaments must be since they are devoid of H) represents definitive evidence that some oxygen burning has occurred in the G292 progenitor. The apparent absence of S or other O-burning products in optical spectra from G292 had been something of a puzzle, since models for the yields from core-collapse SNe all predict from 0.04 to 0.2  $M_\odot$  of S (e.g. Rauscher et al. 2002).

An analysis of the abundances in filaments composed entirely of heavy elements represents a challenge beyond the scope of this paper; nevertheless, the detection of only relatively faint  $[\text{S II}]$  emission in a small minority of G292’s filaments clearly indicates that S is not a prominent constituent in the optical filaments of this SNR. Either there has been only a

---

<sup>4</sup>The 4959 Å and 5007 Å lines in the NGC 4449 SNR are so broad that they cannot be resolved. Note also that Blair et al. (1983) used a distance of 5 Mpc and thus found even higher values for the luminosity.

little oxygen burning, or most of the O-burning products have yet to be excited. Comparing G292 with other O-rich SNRs, only two of these have strong [S II] lines in their optical spectra: Cas A (e.g. Chevalier & Kirshner 1978; Fesen 2001) and 0540–69.3 in the Large Magellanic Cloud (Dopita & Tuohy 1984; Kirshner et al. 1989). In the other members of this small society—Puppis A (Winkler & Kirshner 1985; Sutherland & Dopita 1995a), N132D in the LMC and 1E0102–7219 in the SMC (e.g. Blair et al. 2000, for both), the very bright SNR in NGC 4449 (Blair et al. 1983), and the remnant of SN1957D in M83 (Long et al. 1989)—[S II] is extremely weak or absent entirely in the ejecta-dominated filaments.

### 4.3. Optical–X-Ray Comparison

Comparison of the optical images with high-resolution X-ray images from *Chandra* (Park et al. 2002) shows little detailed correspondence in features. The brightest optical feature, filament 1 where we obtained our spectrum, has no exact X-ray counterpart; it lies  $\sim 30''$  north of the eastern end of the bright equatorial X-ray belt. This X-ray belt does not show enhanced abundances, and Park et al. (2002) have interpreted it as a region where the primary supernova shock is encountering a ring of circumstellar material, seen approximately edge-on. The proximity of such a bright, ejecta-dominated filament to one end of this projected ring may result from a strong reverse shock, produced indirectly by the encounter with the circumstellar ring, propagating into ejecta expanding roughly transverse to our line of sight. The low radial velocity observed for this filament,  $v_r \approx 100 \text{ km s}^{-1}$ , is consistent with near-transverse motion.

Park et al. (2002) show equivalent-width (EW) maps for strong X-ray lines of several metals. For oxygen, the highest equivalent widths are found in a complex within the south-east quadrant of G292. The largest number of O-rich optical filaments are located along a broad arc extending through this quadrant roughly from NNE to SSW (Fig. 1). The Ne (He  $\alpha$ ) and Mg X-ray EW maps also show strong emission along a similar arc. This suggests that pure ejecta fragments similar in composition to the ones we now observe have provided the material for the X-ray plasma in this region.

The *Chandra* data partially complement the optical picture of oxygen-burning products inhomogeneously distributed around G292. The Park et al. (2002) EW map for Si shows a string of prominent X-ray knots extending almost two-thirds of the way across the northern portion of the shell. The two optical filaments where the S/O ratio is highest are both found in this general region. Filament 4 lies near the center of a relatively bright X-ray feature, designated as Region 5 by Park et al. (2004) who found this region to be relatively more enhanced in Si and S than other portions of the SNR. Our filament 3 lies about  $40''$  to

the NW, near the edge of another X-ray complex. Fig. 8 shows a detailed optical/X-ray comparison for this portion of G292. On the version of the *Chandra* image by Gonzalez & Safi-Harb (2003), filaments 4 and 3 are located within their regions 16 and 17, respectively. These contribute to the global abundances they calculated, but they did not report line fluxes or abundance estimates for individual regions.

A particularly interesting set of O-rich filaments is at the extreme south, outside the field of the *Chandra* ACIS image and at the extreme edge of X-ray emission detected from the *ROSAT* HRI, as pointed out in § 2. Fragments of ejecta launched in this direction have traveled farther than any others, so these are probably the fastest such fragments in G292. It appears that the primary shock is encountering a low-density region to the south, leading to more rapid expansion in this direction. Perhaps pre-supernova mass loss has swept out the ISM in this direction, perpendicular to the equatorial ring seen in X-rays. One might suspect a bipolar flow, leading to similar phenomena to the north, but as yet there is no evidence for any emission beyond the near-circular northern portion of the shell. It would be interesting to obtain optical spectra of one or more of the extreme southern filaments and to investigate the X-ray structure here in more detail than can be possible with the *ROSAT* data.

It is interesting to compare the total X-ray luminosity of G292 with that in [O III]. Seward et al. (2005) give values for the X-ray flux based on the *Chandra* ACIS data, viz.  $F_{0.3-2.1 \text{ keV}} = 1.80 \times 10^{-10} \text{ ergs cm}^{-2} \text{ s}^{-1}$ , based on fits using a multi-component model with the absorption column density fixed at  $N_H = 6.16 \times 10^{21} \text{ cm}^{-2}$ . As we argue in §4.1, a column of  $3.3 \times 10^{21} \text{ cm}^{-2}$  is more consistent with all the data for G292. It is not a simple matter to adjust the absorption, since changing  $N_H$  would change other parameters of the fit, but to first order we estimate that the lower absorption would give an unabsorbed flux of  $F_0 \approx 8 \times 10^{-10} \text{ ergs cm}^{-2} \text{ s}^{-1}$ , and an X-ray luminosity  $L_{0.3-2.1 \text{ keV}} \approx 3 \times 10^{36} d_6^2 \text{ ergs s}^{-1}$ , roughly 20 times the luminosity in [O III]  $\lambda$  5007. Comparing G292 with the extraordinary SNR in NGC 4449, Patnaude & Fesen (2003) find for the latter  $L_X = 2.4 \times 10^{36} \text{ ergs s}^{-1}$ , just under half its luminosity in [O III].<sup>5</sup> The [O III]/X-ray luminosity ratio for G292 is probably more typical of O-rich SNRs, but it would be interesting to do a quantitative comparison for others.

---

<sup>5</sup>The X-ray flux and luminosity given by Patnaude & Fesen (2003) are for energy range 0.5–2.1 keV, slightly different from the one used by Seward et al. (2005) for G292.

#### 4.4. Filament Morphology—Rayleigh-Taylor Fingers

The most striking feature of the outer filaments in G292 is that most of them display an elongated, finger-like morphology directed generally outward from the center of the remnant. A common feature of two- and three-dimensional hydrodynamic models for core-collapse supernovae is Rayleigh-Taylor instabilities, which form at interfaces between layers of different composition as the supernova shock pushes outward through the outer core of the progenitor (e.g., Fryxell et al. 1991; Burrows et al. 1995; Nagataki et al. 1998; Kifonidis et al. 2000, 2003). These instabilities produce mixing of material from different layers, as observed in SN1987A (e.g., Arnett et al. 1989; McCray 1993; Wang et al. 2002) and eventually may lead to SNR filaments of highly varied composition, as in Cas A (e.g., Chevalier & Kirshner 1978; Reed et al. 1995; Hurford & Fesen 1996; Fesen 2001). The geometry of most of the outer filaments in G292 is very suggestive of Rayleigh-Taylor instabilities: thin, irregular fingers oriented radially, as illustrated by several examples shown in detail in Fig. 9, taken from locations indicated in Fig. 10.<sup>6</sup> The arrows in each panel of the figure are directed toward the geometric center of the outer radio shell, as defined by Gaensler & Wallace (2003):  $\alpha(2000) = 11^{\text{h}}24^{\text{m}}34^{\text{s}}.2$ ,  $\delta(2000) = -59^{\circ}15'54''$ . (The pulsar is located about  $45''$  to the SE relative to this center, but it could well be moving rapidly, as Hughes et al. 2001, have noted.) These filaments could have originated as R-T fingers, formed when the shock pushed outward through the oxygen zone in the early stages of the supernova explosion, that have been ballistically expanding since. The ejecta clumps would have only recently become visible, once they entered the reverse shock and became excited. Blondin & Ellison (2001) have shown that the fingers should stay near the forward shock front throughout the time that the reverse shock is in the power-law portion of the ejecta density profile—which can extend up to several thousand years.

### 5. Summary

We have obtained the first narrow-band CCD images to cover the entirety of the oxygen-rich SNR G292.0+1.8 and have also obtained a long-slit spectrum from a single particularly interesting position chosen for its strong contrast as seen in [O III] and [S II] images. Our

---

<sup>6</sup>Ghavamian et al. (2005) have suggested that the scalloped morphology of the bright spur filament may result from R-T instabilities that have resulted from the recent encounter of a reverse shock with an overdense shell of ejecta, and they have noted a similarity to filaments in Cas A (Fesen 2001). Our discussion here refers primarily to the outer filaments, whose finger-like geometry may be a remnant of R-T instabilities during the explosion.

findings can be briefly summarized as follows:

1. The [O III] filaments are widespread throughout much of the G292 shell, including a few very near the outer edge of the radio/X-ray shell. All the filaments show no  $H\alpha$  emission and thus appear to be fragments of supernova ejecta, the same conclusion reached by previous studies for filaments in the central region of G292. The filaments at the shell perimeter would seem to be bullets of ejecta that have nearly caught up to the primary shock.

2. We have discovered in our images a few filaments that emit in [S II] in addition to oxygen lines, but that still show no  $H\alpha$ . We have confirmed one of these spectroscopically. These [S II] filaments represent the first evidence for products of oxygen burning in the fragments of pure supernova ejecta in G292. Clearly some oxygen burning must have occurred either hydrostatically in the G292 progenitor or explosively during the supernova, but the paucity of [S II] filaments suggests either that O-burning was not extensive or that most O-burning products have yet to be excited.

3. Most of the [O III] filaments, especially those outside the central region, are radially oriented, pencil-like structures. This is the structure that hydrodynamic simulations for core-collapse supernovae show developing in the outer portion of the progenitor core as a result of Rayleigh-Taylor instabilities. We suggest that the present ejecta "bullets" seen optically may trace their origins back to these features that developed during the explosion.

4. The extinction to G292 is probably equivalent to  $E(B-V) = 0.6$  mag, or  $A(V) = 1.9$  mag, significantly less than has been used in previous discussions of the optical emission from G292. The lower extinction is more consistent both with X-ray and radio measures for the hydrogen column density and with models for the optical emission from a shocked metal-rich gas.

5. The integrated [O III] flux from G292 is  $F_{5007} = 5.4 \times 10^{-12}$  ergs cm $^{-2}$  s $^{-1}$ . This value, with a distance of 6 kpc and our adopted value for the extinction, implies  $L_{5007} = 1.6 \times 10^{35}$  ergs s $^{-1}$ , approximately 20 times smaller than the X-ray luminosity. This is dramatically different from the extraordinary SNR in NGC 4449, which has an [O III] luminosity roughly twice that in X-rays. It would be interesting to obtain similar comparisons for other O-rich SNRs.

The status of G292.0+1.8 as one of only a handful of oxygen-rich SNRs, and especially the fact that it remains unique in displaying all the features expected to result from a core-collapse supernova, makes it an object of continuing interest for further study in all wavelength bands.

We gratefully acknowledge the outstanding support, typical of the mountain staff at CTIO, during the observations that yielded the new data reported here. Several undergraduate students made important contributions at various stages: Becky Walldroff assisted in the acquisition of the spectroscopic data; Sarah Kate May carried out the initial spectroscopic data reduction; and Claudine Reith assisted in acquiring and processing the image data. Comments from Jack Hughes and from the anonymous referee have been valuable in preparing the final version of this paper. This work has been made possible through the financial support from the NSF, through grant AST-0307613 to P.F.W., and from NASA, through grant NAG 5-8020 to P.F.W. and *Chandra* grants GO0-1120X and GO1-2058A to K.S.L. Additional support for astrophysics research at Middlebury College has been provided by the W.M. Keck Foundation through the Keck Northeast Astronomy Consortium.

## REFERENCES

- Arnett, D. 1996, *Supernovae and Nucleosynthesis* (Princeton, NJ: Princeton U. Press)
- Arnett, W. D., Bahcall, J. N., Kirshner, R. P., & Woosley, S. E. 1989, *ARA&A*, 27, 629
- Blair, W. P., Kirshner, R. P., & Winkler, P. F. 1983, *ApJ*, 272, 84
- Blair, W. P., Morse, J. A., Raymond, J. C., Kirshner, R. P., Hughes, J. P., Dopita, M. A., Sutherland, R. S., Long, K. S., & Winkler, P. F. 2000, *ApJ*, 537, 667
- Blair, W. P., Raymond, J. C., Danziger, J., & Matteucci, F. 1989, *ApJ*, 338, 812
- Blondin, J. M. & Ellison, D. C. 2001, *ApJ*, 560, 244
- Burrows, A., Hayes, J., & Fryxell, B. A. 1995, *ApJ*, 450, 830
- Camilo, F., Manchester, R. N., Gaensler, B. M., Lorimer, D. R., & Sarkissian, J. 2002, *ApJ*, 567, L71
- Cardelli, J. A., Clayton, G. C., & Mathis, J. S. 1989, *ApJ*, 345, 245
- Chevalier, R. A. 2005, *ApJ*, 619, 839
- Chevalier, R. A. & Kirshner, R. P. 1978, *ApJ*, 219, 931
- Dopita, M. A. & Tuohy, I. R. 1984, *ApJ*, 282, 135
- Fesen, R. A. 2001, *ApJS*, 133, 161

- Fryxell, B., Arnett, D., & Mueller, E. 1991, *ApJ*, 367, 619
- Gaensler, B. M. & Wallace, B. J. 2003, *ApJ*, 594, 326
- Gaustad, J. E., McCullough, P. R., Rosing, W., & Van Buren, D. 2001, *PASP*, 113, 1326
- Ghavamian, P., Hughes, J. P., & Williams, T. B. 2005, *ApJ*, 635, 365
- Gonzalez, M. & Safi-Harb, S. 2003, *ApJ*, 583, L91
- Goss, W. M., Shaver, P. A., Zealey, W. J., Murdin, P., & Clark, D. H. 1979, *MNRAS*, 188, 357
- Hamuy, M., Walker, A. R., Suntzeff, N. B., Gigoux, P., Heathcote, S. R., & Phillips, M. M. 1992, *PASP*, 104, 533
- Hughes, J. P. & Singh, K. P. 1994, *ApJ*, 422, 126
- Hughes, J. P., Slane, P. O., Burrows, D. N., Garmire, G., Nousek, J. A., Olbert, C. M., & Keohane, J. W. 2001, *ApJ*, 559, L153
- Hughes, J. P., Slane, P. O., Park, S., Roming, P. W. A., & Burrows, D. N. 2003, *ApJ*, 591, L139
- Hunter, D. A., van Woerden, H., & Gallagher, J. S. 1999, *AJ*, 118, 2184
- Hurford, A. P. & Fesen, R. A. 1996, *ApJ*, 469, 246
- Kifonidis, K., Plewa, T., Janka, H.-T., & Müller, E. 2000, *ApJ*, 531, L123
- Kifonidis, K., Plewa, T., Janka, H.-T., & Müller, E. 2003, *A&A*, 408, 621
- Kirshner, R. P., Morse, J. A., Winkler, P. F., & Blair, W. P. 1989, *ApJ*, 342, 260
- Long, K. S., Blair, W. P., & Krzeminski, W. 1989, *ApJ*, 340, L25
- McCray, R. 1993, *ARA&A*, 31, 175
- Mills, B. Y., Slee, O. B., & Hill, E. R. 1961, *Australian Journal of Physics*, 14, 497
- Milne, D. K. 1969, *Australian Journal of Physics*, 22, 613
- Murdin, P. & Clark, D. H. 1979, *MNRAS*, 189, 501
- Nagataki, S., Shimizu, T. M., & Sato, K. 1998, *ApJ*, 495, 413



- Park, S., Hughes, J. P., Slane, P. O., Burrows, D. N., Roming, P. W. A., Nousek, J. A., & Garmire, G. P. 2004, *ApJ*, 602, L33
- Park, S., Roming, P. W. A., Hughes, J. P., Slane, P. O., Burrows, D. N., Garmire, G. P., & Nousek, J. A. 2002, *ApJ*, 564, L39
- Patnaude, D. J. & Fesen, R. A. 2003, *ApJ*, 587, 221
- Predehl, P. & Schmitt, J. H. M. M. 1995, *A&A*, 293, 889
- Rauscher, T., Heger, A., Hoffman, R. D., & Woosley, S. E. 2002, *ApJ*, 576, 323
- Reed, J. E., Hester, J. J., Fabian, A. C., & Winkler, P. F. 1995, *ApJ*, 440, 706
- Seward, F., Slane, P., Smith, R., Gaetz, T., Koo, B.-C., & Lee, J.-J. 2005, Chandra Supernova Remnant Catalog, <http://snrcat.cfa.harvard.edu/>
- Sutherland, R. S. & Dopita, M. A. 1995a, *ApJ*, 439, 365
- . 1995b, *ApJ*, 439, 381
- Tuohy, I. R., Burton, W. M., & Clark, D. H. 1982, *ApJ*, 260, L65
- Wang, L., Wheeler, J. C., Höflich, P., Khokhlov, A., Baade, D., Branch, D., Challis, P., Filippenko, A. V., Fransson, C., Garnavich, P., Kirshner, R. P., Lundqvist, P., McCray, R., Panagia, N., Pun, C. S. J., Phillips, M. M., Sonneborn, G., & Suntzeff, N. B. 2002, *ApJ*, 579, 671
- Winkler, P. F. & Kirshner, R. P. 1985, *ApJ*, 299, 981
- Winkler, P. F., Roberts, P. F., & Kirshner, R. P. 1991, in *Supernovae. The Tenth Santa Cruz Workshop in Astronomy and Astrophysics*, held July 9-21, 1989, Lick Observatory. Editor, S.E. Woosley; Publisher, Springer-Verlag, New York, 1991. LC # QB856 .S26 1989. ISBN # 0387970711. P.652, 1991, 652–+
- Woosley, S. E., Heger, A., & Weaver, T. A. 2002, *Reviews of Modern Physics*, 74, 1015
- Zacharias, N., Urban, S. E., Zacharias, M. I., Hall, D. M., Wycoff, G. L., Rafferty, T. J., Germain, M. E., Holdenried, E. R., Pohlman, J. W., Gauss, F. S., Monet, D. G., & Winter, L. 2000, *AJ*, 120, 2131

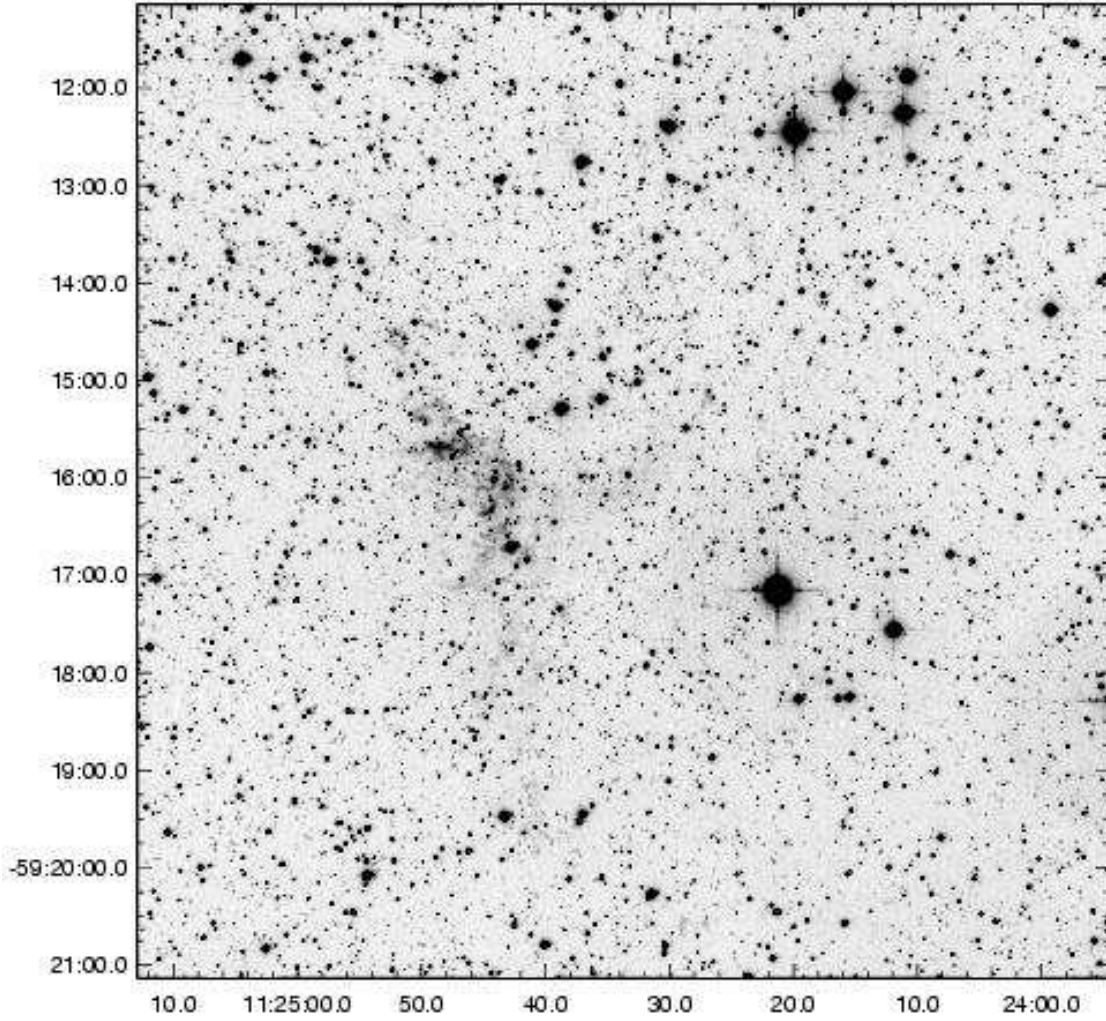


Fig. 1a.— SNR G292.0+1.8 in the light of [O III]. The field is 10' square, with N up, and E left, and is identical in Figures 1–4.

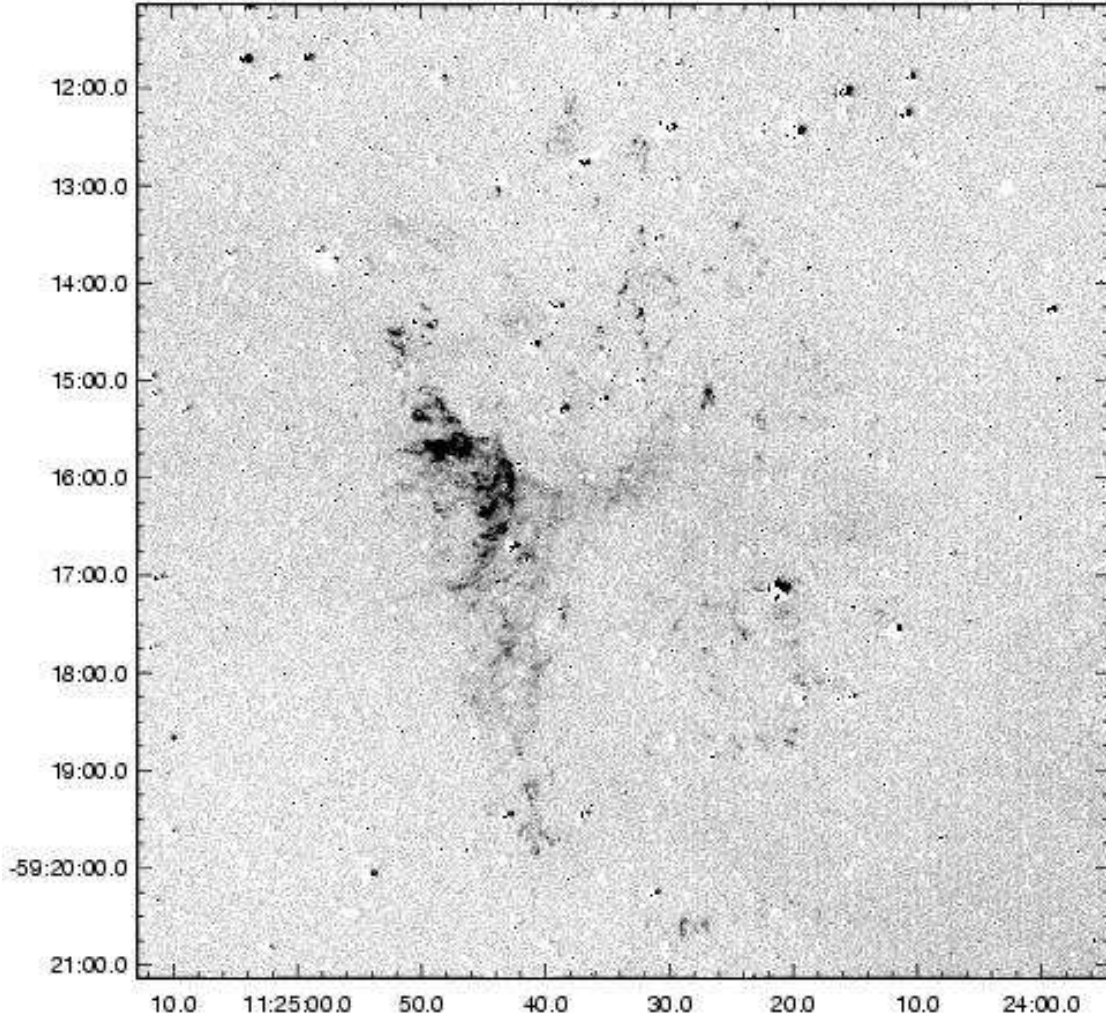


Fig. 1b.— SNR G292.0+1.8 in the light of [O III] (same image as Fig. 1a) with a matched continuum image subtracted to reveal the nebular features more clearly.

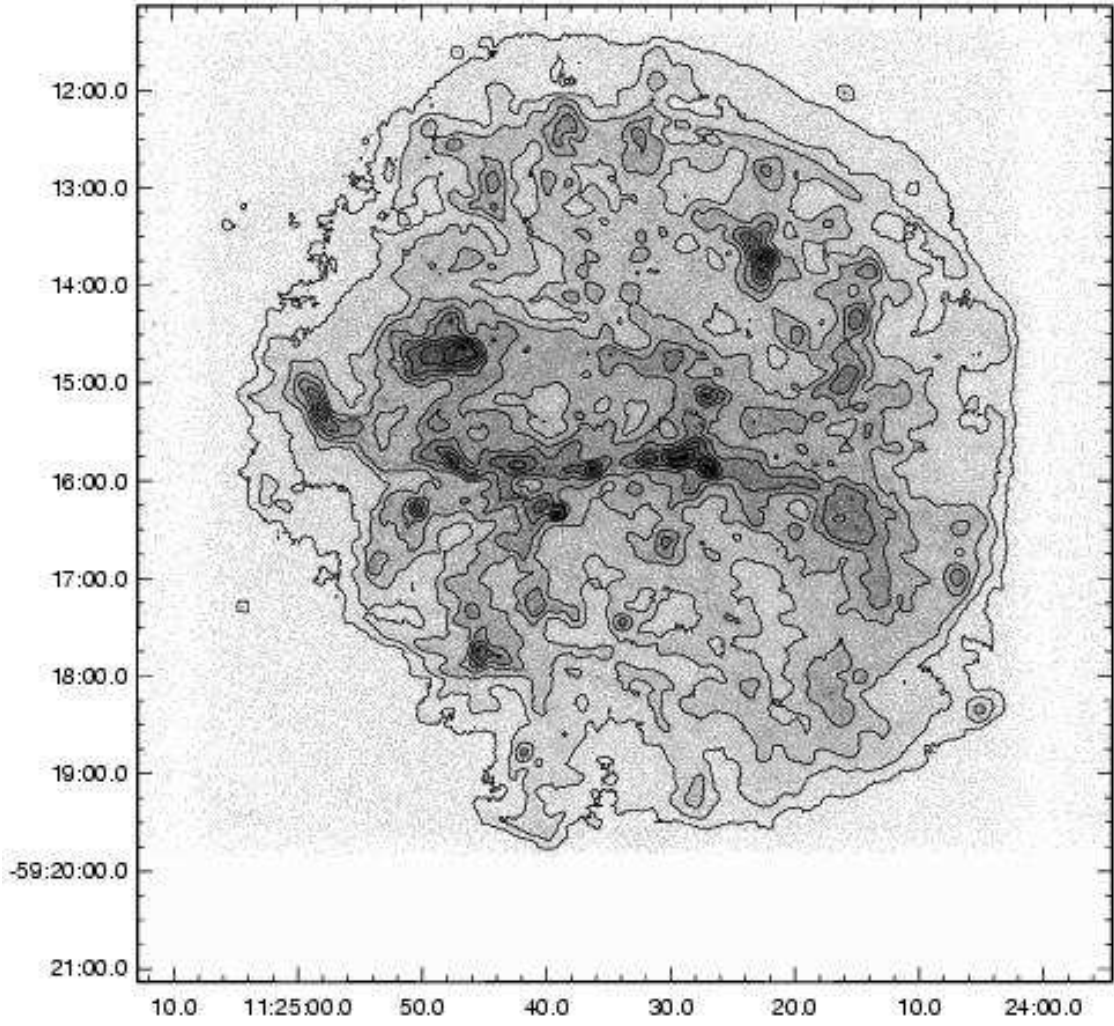


Fig. 2a.— *Chandra* ACIS image of the SNR G292.0+1.8 (Park et al. 2002), with contours added. The field is identical to that in Fig. 1, but the southern edge of the ACIS chip is at  $\delta(2000) \approx -59^\circ 19' 45''$ .

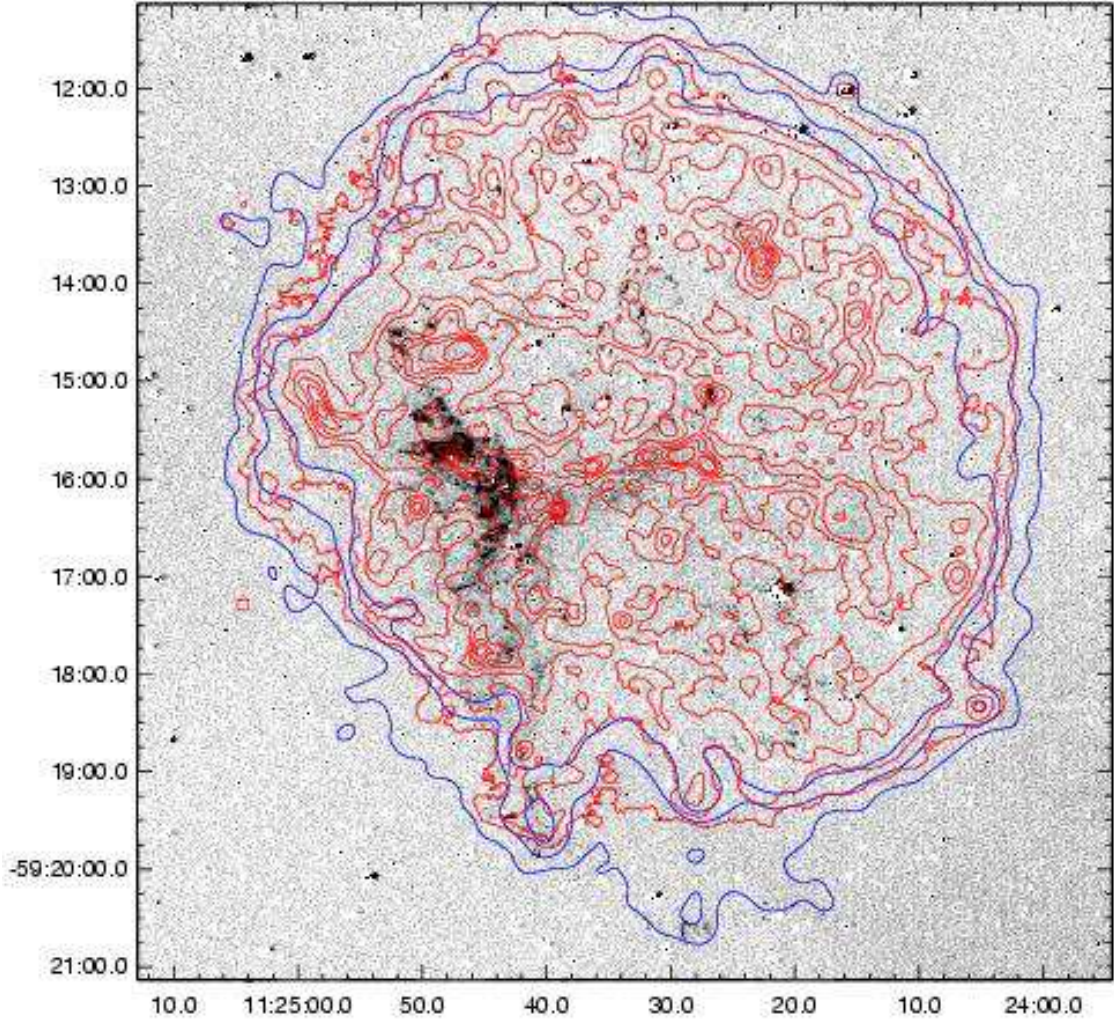


Fig. 2b.— The same continuum-subtracted [O III] image shown in Fig. 1b, with the ACIS contours shown in red. The outermost contours of a ROSAT HRI image of G292 are also shown, in blue.



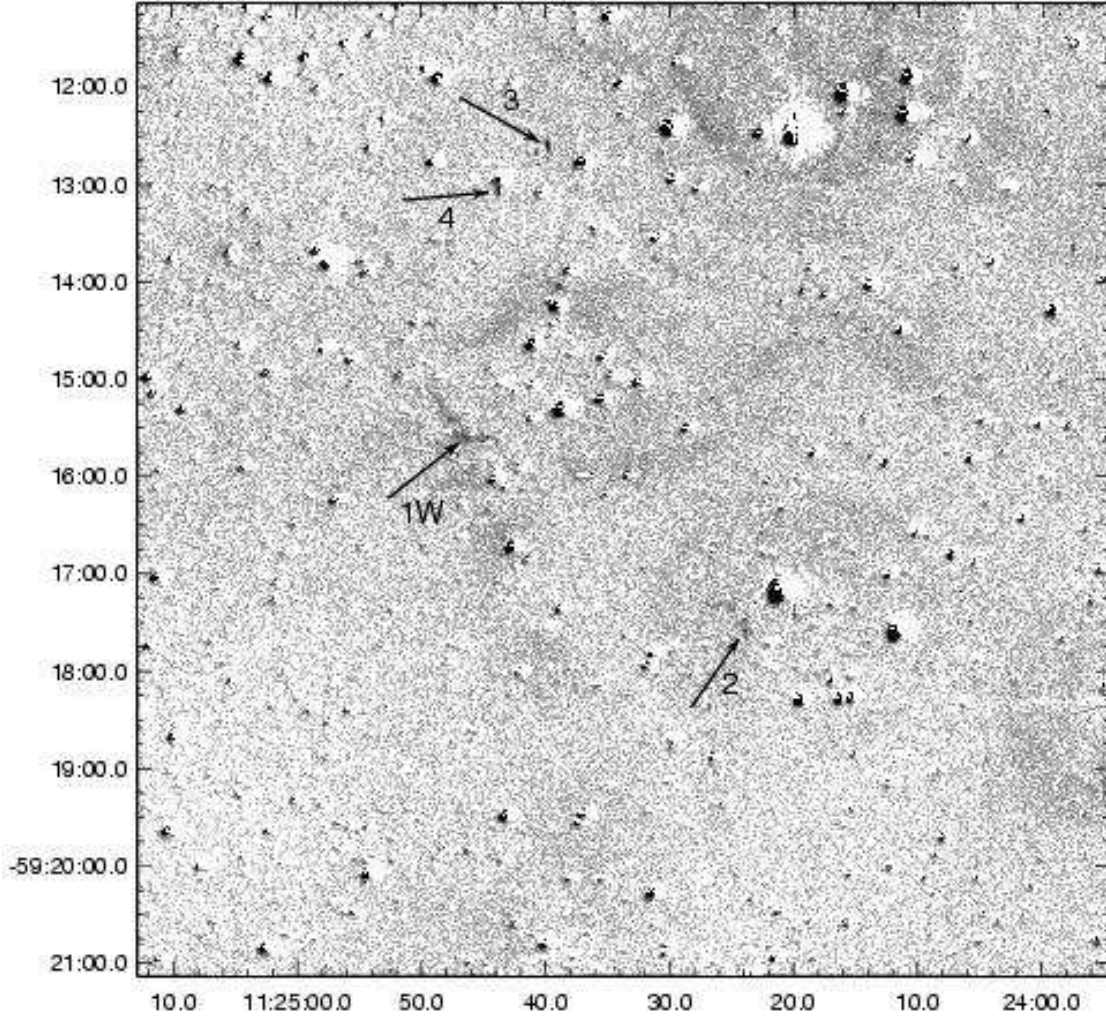


Fig. 3.— SNR G292.0+1.8 in the light of [S II]  $\lambda\lambda$  6716,6731, with a matched red continuum image subtracted. The arrows indicate the locations of four groups of [S II] filaments. Reflections from both the [S II] and continuum filters has left significant residuals from bright stars. The field is identical to that in Fig. 1.

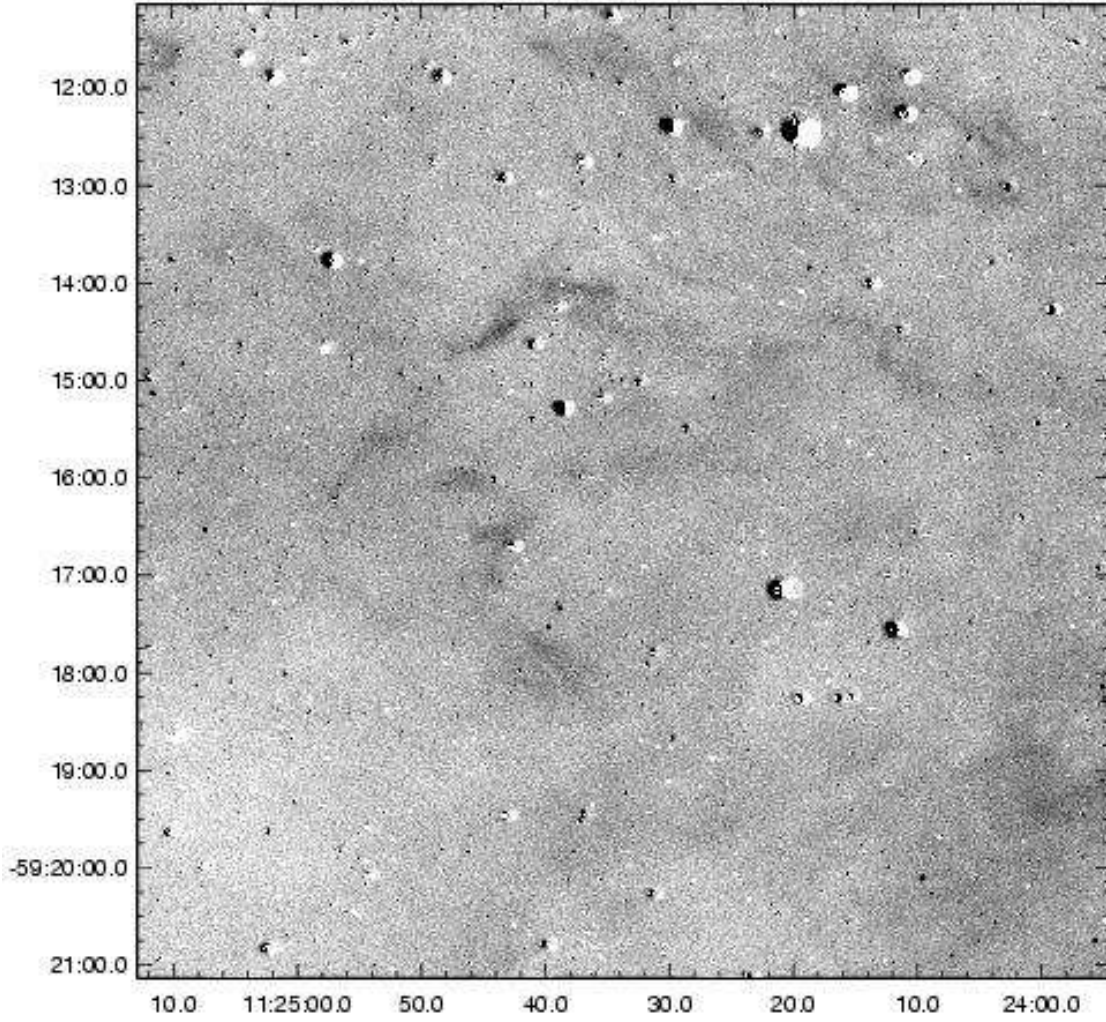


Fig. 4.— SNR G292.0+1.8 in the light of  $H\alpha$  with a matched red continuum image subtracted. Note the absence of any emission from the small filaments seen in  $[O\ III]$  and/or  $[S\ II]$ . The field is identical to that in Fig. 1.

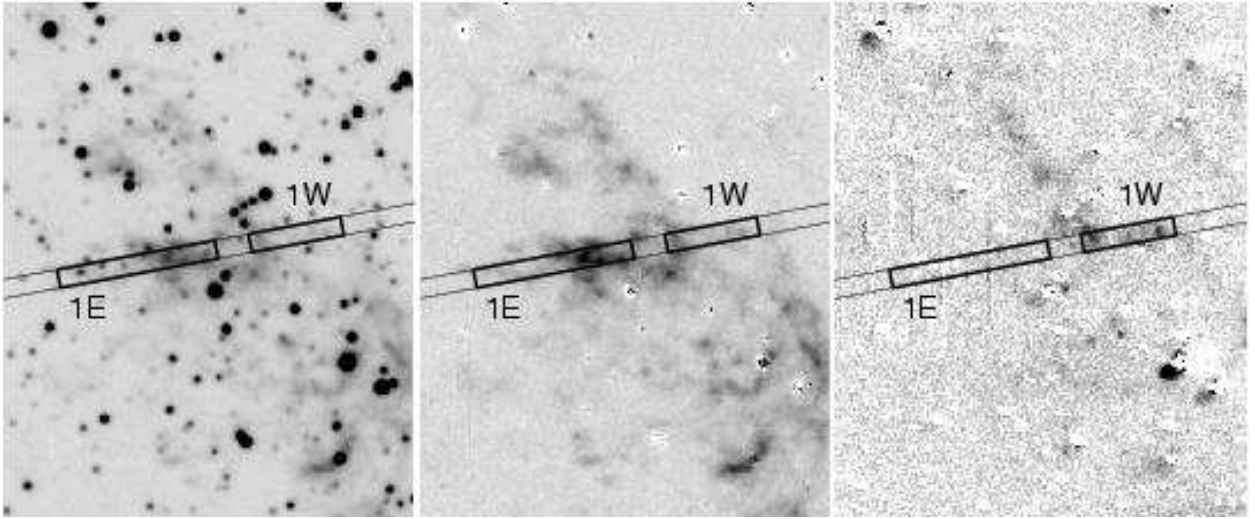


Fig. 5.— The slit position for our long-slit spectrum (Fig. 6) of G292.0+1.8 is shown on identical sections of three images: (*left*) [O III], (*center*) continuum-subtracted [O III], and (*right*) continuum-subtracted [S II]. One-dimensional spectra (Fig. 7) were extracted from the two regions indicated by the heavier boxes: 1E includes the brightest [O III] filament in G292 (the northern portion of the “Spur”); 1W is a western extension of this filament and includes the brightest [S II] filament known at the time our spectrum was obtained. The field shown is  $80'' \times 100''$ .



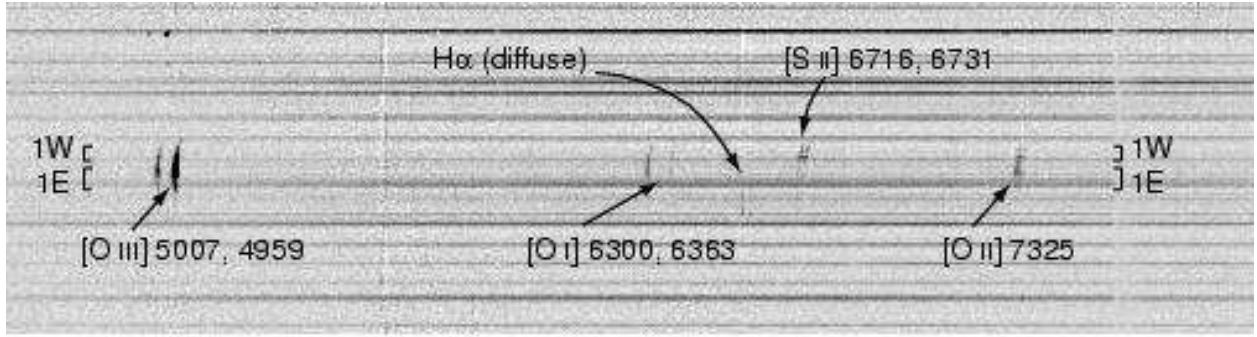


Fig. 6.— Deep long-slit spectrum G292.0+1.8 with the slit oriented near east-west along the bright filament 1, as shown in Fig. 5. This 2-D spectrum is from one of our 3 overlapping spectral ranges. The oxygen lines are all strongest in the main eastern portion (1E) of the filament, while [S II] emission is strongest in the western extension (1W). The filamentary emission shows a distinct curvature resulting from a radial velocity gradient of  $\sim 500 \text{ km s}^{-1}$  along the filament. The  $\text{H}\alpha$  emission shows no such velocity variation, and so has been largely removed in the sky subtraction further indication that the filaments themselves are virtually devoid of H. The two 1-D spectra shown in Fig. 7 were obtained by artificially removing the curvature, followed by extraction from regions 1E and 1W.

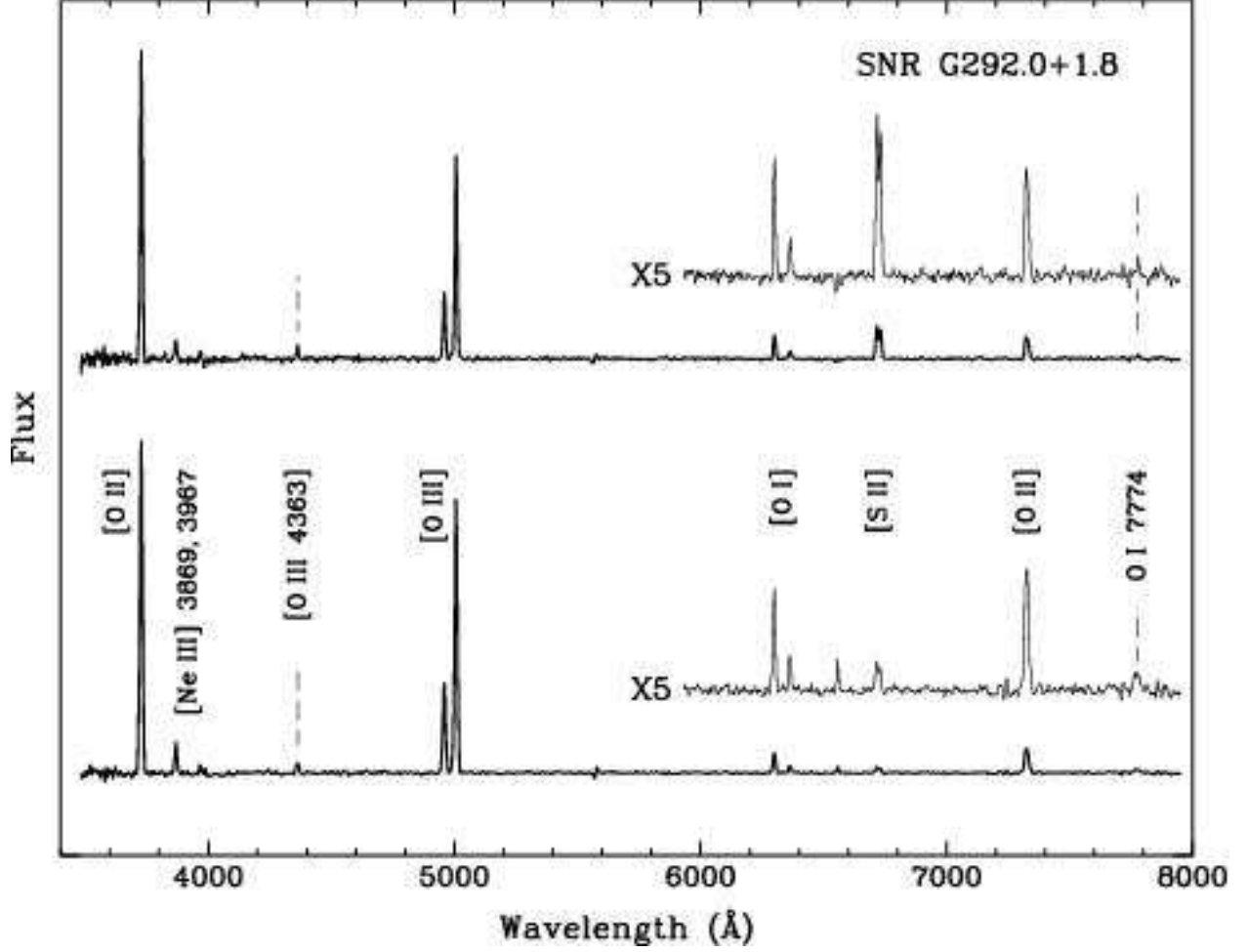


Fig. 7.— These combined 1-D extracted spectra from two regions along the slit (filament 1E below, 1W above) show similar relative strengths from [O I], [O II], and [O III], but the [S II] lines are 8 times stronger (relative to [O II]) in the upper spectrum. Note also the faint line from permitted O I, which results from  $\text{O}^+$  winning out over  $\text{H}^+$  in recombination. The long-wavelength ends of both spectra are repeated in the insets with the vertical scale magnified by a factor of 5.

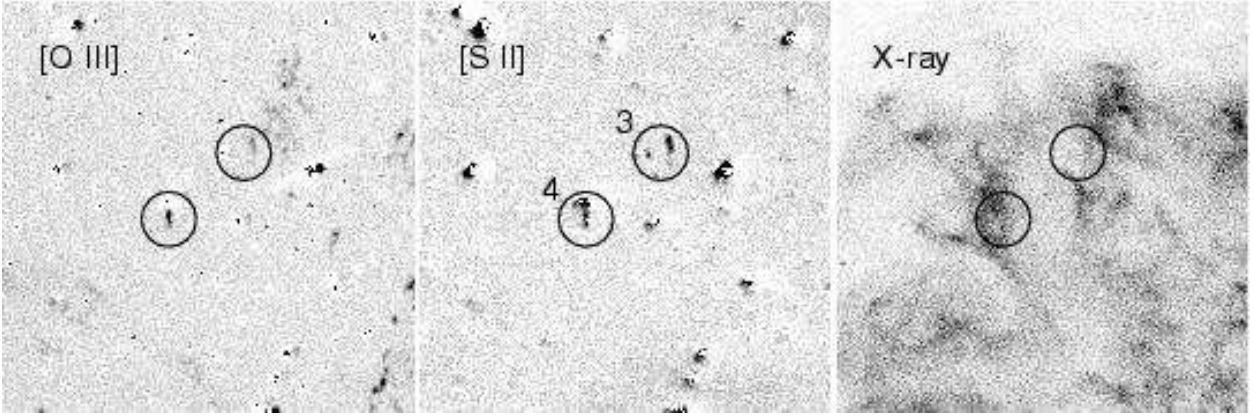


Fig. 8.— This  $2'.5$  square section from the [O III], [S II], and *Chandra* ACIS X-ray images of G292.0+1.8 shows the filament (No. 3) with the highest optical [S II]/[O III] ratio. In the same circle with filament 3 is another tiny S-rich knot,  $8''$  to the east, which also has high [S II]/[O III]. Filament 4 coincides with an X-ray feature where Park et al. (2004) found Si and S to be more enhanced than anywhere else in G292. The circles have a diameter of  $20''$  and the numbers on the [S II] panel are the same as in Fig. 3.

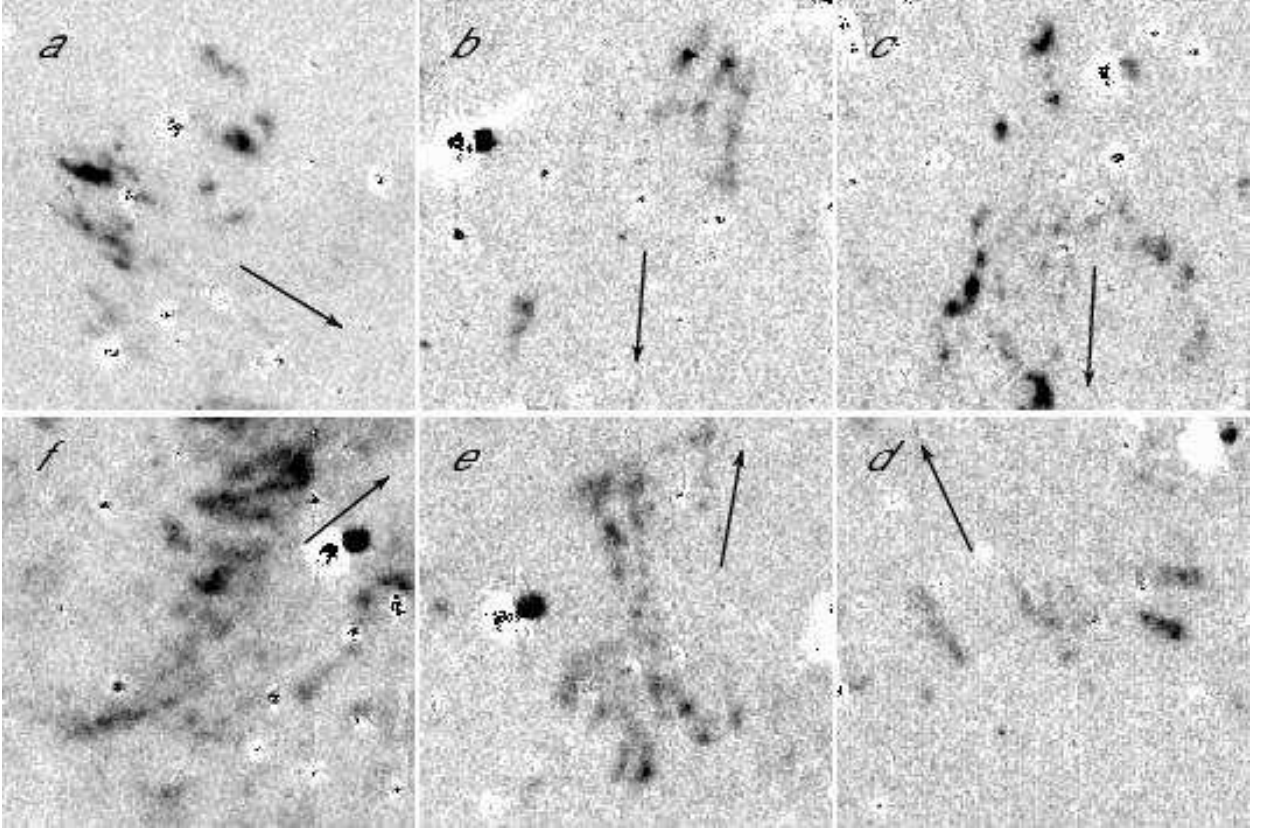


Fig. 9.— These enlargements of the continuum-subtracted [O III] image (the same as that shown in Fig. 1b) show details of numerous ejecta filaments in G292.0+1.8, almost all of which display a thin, pencil-like morphology that suggests an origin as Rayleigh-Taylor fingers. The arrows are all directed toward the geometric center of the radio shell, as given by Gaensler & Wallace (2003); note that most of the fingers are oriented in a near-radial direction. Each of the panels is exactly  $1'$  square, and are taken from locations *a-f* indicated in Fig. 10.

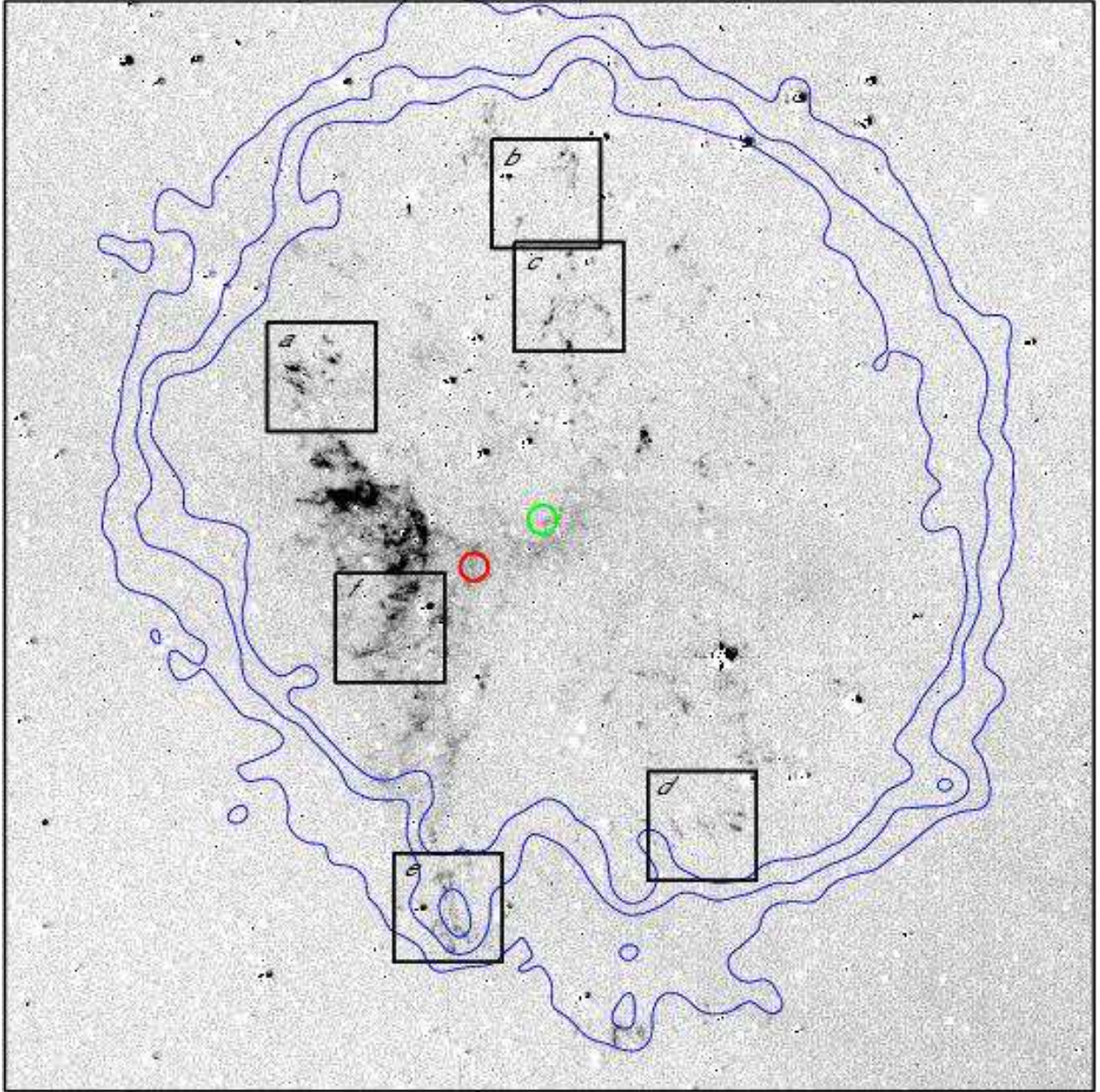


Fig. 10.— The location from which each of the panels *a-f* in Fig. 9 was taken is indicated by the corresponding field on this continuum-subtracted [O III] image of G292.0+1.8. The red circle indicates the position of the pulsar PSR J1124–5916, and the green circle indicates the geometric center of the radio shell as given by Gaensler & Wallace (2003). As an additional reference, the outer X-ray contours (from the *ROSAT* HRI, the same as shown in Fig. 2b) are shown in blue.

Table 1. Imaging Observations of G292.0+1.8.

| Designation                        | Filter          |                       | Velocity Range <sup>b</sup> |   |       | Exposure<br>(s) |
|------------------------------------|-----------------|-----------------------|-----------------------------|---|-------|-----------------|
|                                    | $\lambda_0$ (Å) | $\Delta\lambda^a$ (Å) | km s <sup>-1</sup>          |   |       |                 |
| [O III] $\lambda$ 5007             | 5008            | 58                    | −1700                       | - | +1800 | 5 × 1000        |
| Green Continuum                    | 5133            | 100                   |                             |   |       | 5 × 500         |
| H $\alpha$                         | 6565            | 24                    | − 450                       | - | + 650 | 3 × 1000        |
| [S II] $\lambda\lambda$ 6716, 6731 | 6728            | 48                    | − 550                       | - | +1600 | 4 × 1000        |
|                                    |                 |                       | −1200                       | - | + 950 |                 |
| Red Continuum                      | 6848            | 94                    |                             |   |       | 5 × 400         |

<sup>a</sup>FWHM.

<sup>b</sup>For [S II], the velocity range is given separately for the 6716 Å and 6731 Å lines.

Table 2. Spectroscopic Observations of G292.0+1.8

| Setup | Grating | Tilt  | Wavelength Coverage<br>(Å) | Filter | Exposure<br>(s) |
|-------|---------|-------|----------------------------|--------|-----------------|
| Blue  | 09      | 13°27 | 3,500–6,900                | —      | $4 \times 1800$ |
| Red   | 32      | 14°10 | 4,560–7,960                | GG420  | $5 \times 1200$ |
| IR    | 32      | 15°66 | 6,600–10,000               | RG610  | $4 \times 1800$ |

Table 3. Observed Emission-Line Fluxes in G292.0+1.8

| Wavelength<br>(Å) | Ion        | Flux <sup>a,b</sup> ([O III] $\lambda$ 5007 = 100) |             | Intensity ([O III] $\lambda$ 5007 = 100)<br>Dereddened, <sup>c</sup> $E(B - V) = 0.6$ |             | Intensity ([O III] $\lambda$ 5007 = 100)<br>Dereddened, <sup>c</sup> $E(B - V) = 0.9$ |             |
|-------------------|------------|--|-------------|---|-------------|---|-------------|
|                   |            | Fil. 1 East  | Fil. 1 West | Fil. 1 East   | Fil. 1 West | Fil. 1 East   | Fil. 1 West |
| 3727              | [O II]     | 117  | 147         | 240   | 302         | 343   | 432         |
| 3869              | [Ne III]   | 10   | 9           | 20  | 18          | 28  | 25          |
| 3967              | [Ne III]   | 2.5  | 3.5         | 4.5   | 6.4         | 6.2   | 8.5         |
| 4363              | [O III]    | 3.6  | 5.3         | 5.3   | 7.8         | 6.4   | 9.4         |
| 4959              | [O III]    | 33   | 32          | 34  | 33          | 34  | 33          |
| 5007              | [O III]    | 100.0  | 100.0       | 100.0   | 100.0       | 100.0   | 100.0       |
| 6300              | [O I]      | 6.9  | 12          | 4.5   | 7.6         | 3.6   | 6.0         |
| 6363              | [O I]      | 2.6  | 3.9         | 1.7   | 2.5         | 1.3   | 2.0         |
| 6563              | H $\alpha$ | < 2  | < 1         | < 1   | < 1         | < 1   | < 1         |
| 6716              | [S II]     | 2.0  | 17          | 1.2   | 9.4         | 0.9   | 7.1         |
| 6731              | [S II]     | 1.3  | 14          | 0.8   | 8.1         | 0.6   | 6.2         |
| 7325              | [O II]     | 14   | 17          | 6.7   | 8.4         | 4.7   | 5.9         |
| 7774              | O I        | (2)  | (2)         | (0.7)   | (0.8)       | (0.5)   | (0.5)       |

<sup>a</sup>For Fil. 1 East,  $F_{5007} = 10.8 \times 10^{-14} \text{ ergs cm}^{-2} \text{ s}^{-1}$ , summed along  $31''$  of the  $3''5$  slit; for Fil. 1 West,  $F_{5007} = 3.5 \times 10^{-14} \text{ ergs cm}^{-2} \text{ s}^{-1}$ , summed along  $19''$  of the same slit.

<sup>b</sup>Values in parentheses have high uncertainty.

<sup>c</sup>The extinction function of Cardelli et al. (1989) with  $A(V)/E(B - V) = 3.1$  was used for the dereddening.